

Non-equilibrium breakdown of quantum Hall state in graphene

Vibhor Singh and Mandar M. Deshmukh*

*Department of Condensed Matter Physics and Materials Science,
Tata Institute of Fundamental Research, Homi Bhabha Road, Mumbai, 400005 India
(Dated: September 11, 2021)*

In this report we experimentally probe the non-equilibrium breakdown of the quantum Hall state in monolayer graphene by injecting a high current density ($\sim 1\text{A/m}$). The measured critical currents for dissipationless transport in the vicinity of integer filling factors show a dependence on filling factor. The breakdown can be understood in terms of inter Landau level (LL) scattering resulting from mixing of wavefunctions of different LLs. To further study the effect of transverse electric field, we measured the transverse resistance between the $\nu = 2$ to $\nu = 6$ plateau transition for different bias currents and observed an invariant point.

PACS numbers: 73.43.-f, 73.63.-b, 71.70.Di

The quantum Hall effect (QHE)¹ has been studied extensively in 2D systems and its equilibrium electron-transport properties are understood to a large extent. The breakdown of the QHE under non-equilibrium conditions due to a high current density has been studied to understand its microscopic origin^{2,3}. There has been a considerable debate in the literature regarding the details of the mechanism of QHE breakdown. The proposed mechanisms include electron heating⁴, electron-phonon scattering^{5,6}, inter and intra Landau level (LL) scattering^{7,8}, percolation of incompressible regions⁹ and the existence of compressible regions in the bulk¹⁰.

Recently QHE has also been observed in graphene¹¹ and studied extensively¹². In this paper we probe the breakdown of the QHE in graphene by injecting a high current density ($\sim 1\text{A/m}$); this results in a large local electric field in the system. The unique band structure of graphene near the Fermi energy ($E = \pm\hbar v_F|k|$, where $v_F \approx 10^6\text{ms}^{-1}$ is the Fermi velocity) gives rise to a ‘relativistic’ QHE. In a magnetic field perpendicular to its plane, the energy spectrum of graphene splits into unequally spaced LLs and is given by $E_n = \text{sgn}(n)\sqrt{(2\hbar c^2 e B|n|)}$, where n is the LL index. When the Fermi level lies between two LLs, the longitudinal resistance (R_{xx}) vanishes and the transverse resistance (R_{xy}) gets quantized to $\frac{h}{(4|n|+2)e^2}$. Further, the presence of transverse electric field mixes the electron and hole wavefunctions and modifies the energy spectrum^{13,14,15}, which is given by $E_n = \text{sgn}(n)\sqrt{(2\hbar c^2 e B|n|)}(1 - \beta^2)^{3/4} - \hbar c\beta k_{\perp}$, where $\beta = E/(cB)$, E is the electric field orthogonal to B , and k_{\perp} is the wave vector in the direction perpendicular to E and B .

The motivation for exploring the breakdown of QHE in graphene is twofold – first, the QHE in graphene is very different from the QHE in a 2DEG system. The LL energy spectrum of 2DEG is equispaced unlike that in graphene. The energy scale set by the cyclotron gap (ΔE_{ν}) in graphene at $B = 10\text{T}$, is much higher ($\sim 1300\text{K}$) than its value for a 2DEG ($\sim 20\text{K}$) at the same magnetic field¹². The mechanism of breakdown in graphene could be the inter-LL scattering due to wavefunction-mixing or possibly entirely different if the

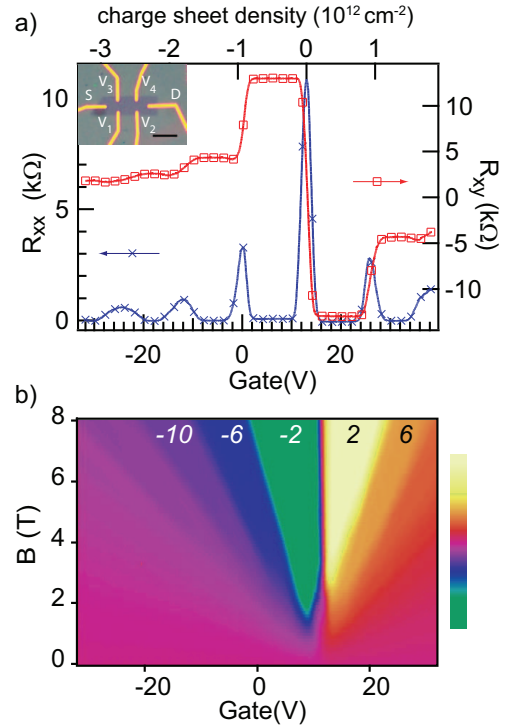


FIG. 1: (color online) a) Line plot of the longitudinal resistance (R_{xx}) and transverse resistance (R_{xy}) for a monolayer graphene device at 300 mK and 9 T. The inset shows an optical microscope image. The scale bar corresponds to $6\ \mu\text{m}$. Probes S and D were used to current bias the device. By using a lock-in technique, probe pairs $V_1 - V_2$ and $V_1 - V_3$ were used to measure R_{xx} and R_{xy} respectively. 50 nA of AC current at 181 Hz was used for these measurements. b) Colorscale plot of R_{xy} , to show the plateaus of varying magnitude clearly, as a function of magnetic field at 300 mK.

lengthscale for variation of the local electric field due to defects is comparable to the magnetic length. In such a situation, ($\beta \geq 1$), a ‘collapse’ of the LL is possible before a longer lengthscale breakdown of QHE¹³. Second, graphene shows room temperature QHE¹⁶ at high magnetic field, therefore understanding the breakdown

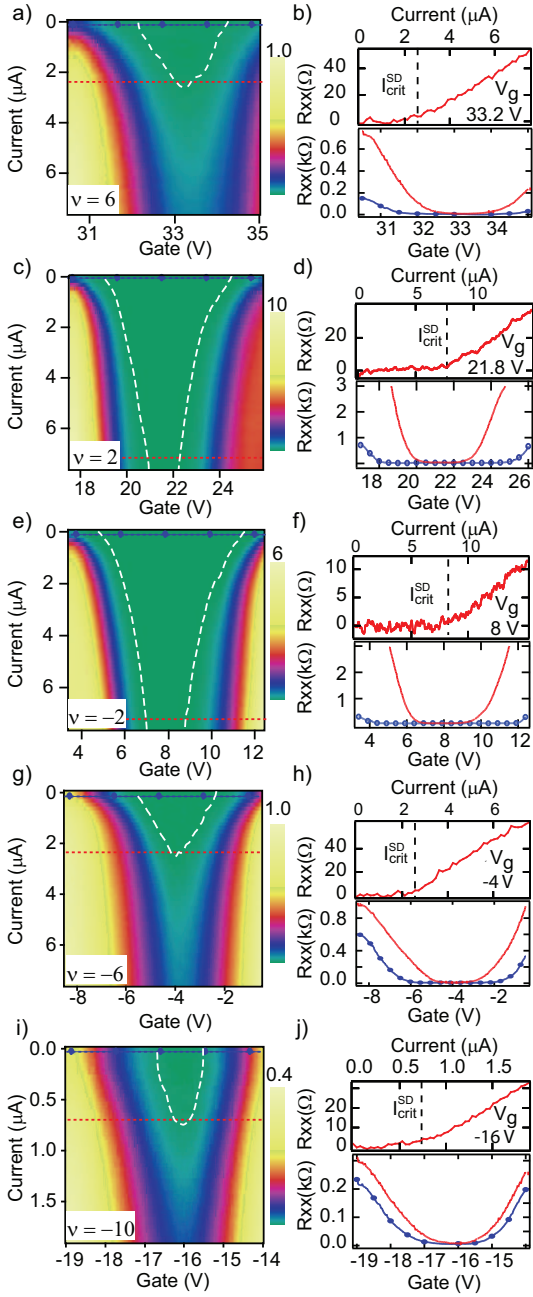


FIG. 2: (color online) Critical current measurements in the vicinity of integer filling factors at 9 T and 300 mK. a, c, e, g and i show the colorscale plot of R_{xx} as a function of I_{DC}^{SD} and V_g near filling factors 6, 2, -2, -6, and -10 respectively. Color bars indicate the resistance in units of $k\Omega$. The white dotted lines on the colorscale plot mark the dissipationless region. The line plots in b, d, f, h and j show slices along the current axis at the gate voltages shown in the figure (top) and two slices (bottom) each for the equilibrium (labeled with solid circles) and non-equilibrium (solid line) biasing conditions. The position of these slices is marked in adjoining colorscale plots (marked a, c, e, g and i).

mechanism can also be useful for metrological resistance standards¹⁷. In addition, the presence of back gate in our devices allows us to change the Fermi level. We can hence probe the QH breakdown away from the integer filling factors without changing the energy spectrum. With these motivations in mind we have probed the breakdown of QHE near the filling factors ($sgn(n)(4|n| + 2)$)^{11,18}, $\nu = -10, -6, -2, 2, 6$ ¹⁹. To better understand the role of high current densities we have modeled the effect of high current using a current-injection model¹⁵; this allows us to explain the experimentally observed transition from neighboring filling factors in terms of an invariant point. We also provide evidence to show that these experimental observations cannot be explained purely on the basis of local electronic heating.

To fabricate monolayer graphene devices in a Hall bar geometry, we have followed the mechanical exfoliation technique^{11,12} on degenerately-doped silicon substrates coated with 300 nm thick SiO_2 . We optically locate the flakes of graphene and pattern electrodes onto them using electron beam lithography. The electrodes are fabricated by depositing 10 nm Cr and 50 nm of Au by thermal evaporation. The degenerately-doped silicon substrate serves as a back-gate to tune the density of carriers by applying a voltage V_g . The inset of Fig.1a shows an optical image of a Hall bar device. In Fig.1a we plot the longitudinal resistance (R_{xx}) and transverse resistance (R_{xy}) at $T = 300$ mK and $B = 9$ T. Filling factors, unique to monolayer graphene ($\nu = \pm 2, \nu = \pm 6$) are clearly seen for both types of carriers in Fig.1a. The mobility of the device shown in the inset is measured to be $\sim 11000 \text{ cm}^2(\text{Vs})^{-1}$ for both types of carriers at 300 mK; by using the semi-classical relation for mean free path (l),²⁰ the measured mobility gives $l = 70$ nm for carrier density $3 \times 10^{11} \text{ cm}^{-2}$. In Fig.1b we plot the evolution of R_{xy} as a function of V_g and magnetic field B . The plateaus in R_{xy} corresponding to $\nu = \pm 2, \pm 6$ and -10 are clearly seen. The Dirac peak for the device is shifted to about 13 V due to unintentional doping, which corresponds to a charge inhomogeneity of $6 \times 10^{11} \text{ cm}^{-2}$. From the two probe resistance measurements at $B = 8$ T, we find that contact resistance is smaller than 700Ω in the QH regime.

To probe the breakdown of QHE, we biased the source-drain probes of our device with DC current (I_{DC}^{SD}) along with a small AC current (50 nA) in the minima of R_{xx} corresponding to filling factors $\nu = \pm 2, \pm 6$ and -10 ¹⁹ at fixed magnetic field. The AC current remains fixed and I_{DC}^{SD} is then varied as a function of V_g in the vicinity of integer ν . The AC signals between the voltage probes V_1 and V_2 and the voltage probes V_1 and V_3 were monitored with a lock-in amplifier to record the values of R_{xx} and R_{xy} respectively. Fig.2 shows the evolution of the R_{xx} minima as function of I_{DC}^{SD} for different filling factors. The line plots show slices of the data in equilibrium and non-equilibrium biasing conditions. In order to interpret the breakdown from the measured experimental data we define a critical current (I_{crit}^{SD}) as the linearly

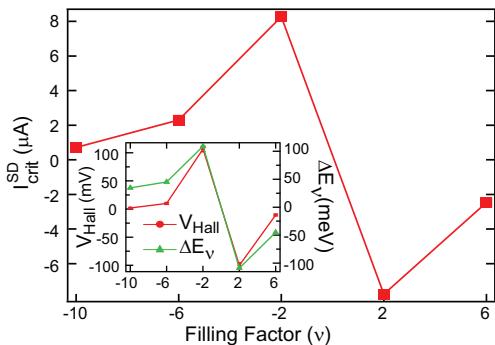


FIG. 3: (color online) Plot of critical current (I_{crit}^{SD}) for different filling factors at $T = 300$ mK and $B = 9$ T. The inset shows the plot of Hall voltage developed at breakdown (V_{Hall} , labeled with circles) and the cyclotron gaps (ΔE_ν) (solid triangles) plotted on right axis as a function of ν .

extrapolated value of I_{DC}^{SD} at zero dissipation²².

We point out the qualitative features of our data – first, with the increase of I_{DC}^{SD} , the width of the dissipationless region reduces, eventually leading to the breakdown. Second, the critical current is ν dependent. Third, on either side of the integer filling factor the boundary of dissipation evolves asymmetrically. In Fig.2a, c, e, g and i for $\nu = 6, 2, -2, -6$ and -10 respectively we see a non-linear evolution of the boundary of dissipation as a function of I_{DC}^{SD} and V_g .

Before discussing details of the data, we address the possible concerns about local heating of the sample that could occur in these studies. We have done control experiment to confirm that heating is not responsible for the key experimental observations; by comparing change of resistance with temperature and due to current. We injected a large DC current through the voltage probes V_1 and V_2 of the Hall bar geometry device to intentionally heat it locally while we simultaneously measured two probe resistance-gate voltage characteristic of the opposite two probes (V_3 and V_4) using a lock-in technique. Then, we observed the evolution of two probe resistance-gate voltage characteristic of the same pair (V_3 and V_4) with temperature while the injected DC current was set to zero. By comparing these two data sets (change of resistance with temperature and due to current), we could estimate that the temperature of the device does not increase beyond 3 K while injecting currents as high as $10 \mu A$. We have also seen an overall asymmetry in the evolution of R_{xx} with the sign of injected current close to integer filling factor. Pure thermal effects cannot explain this asymmetry. Additionally, cyclotron gaps in graphene are large and thermal effects cannot completely suppress the electric field induced effect. Also, superior thermal conductivity of graphene²¹ is likely to suppress any local thermal hot-spot formation.

In order to understand the mechanism of the breakdown we examine the dependance of I_{crit}^{SD} on ν . Fig.3 shows the plot of I_{crit}^{SD} for various filling factors ν in-

dicating that I_{crit}^{SD} decreases with $|\nu|$. The inset shows the plot of two relevant quantities, Hall voltage, $V_{Hall} = I_{crit}^{SD} \times \frac{h}{ve^2}$, and ΔE_ν as a function of ν . There is a correlation between V_{Hall} and ΔE_ν , which can be explained by considering inter LL scattering. The origin of the inter-LL scattering is likely to be the strong local electric field that mixes the electron and hole wavefunctions^{13,14,15} providing a finite rate for inelastic transitions. The energy for the transitions is provided by the transverse electric field parallel to the electron trajectory. This results in inelastic scattering between LLs leading to a breakdown of the dissipationless QH state⁷. Similar inter-LL scattering mechanisms have been used to explain the breakdown of the QHE in a 2DEG, in samples of width less than $10 \mu m$ and moderate mobility^{2,7,22}. The electric field for inter-LL (E_{LL}) scattering can be estimated to be that field where the quasiparticle can pick up an energy corresponding to the LL separation within few cyclotron radii (r_c) i.e. $eE_{LL} \sim \Delta E_\nu / r_c \approx 10^6$ V/m. This is much higher than the experimentally observed electric fields. However, Martin *et al.*²³ found a much shorter lengthscale associated with the charge inhomogeneity (~ 150 nm). The presence of a charge inhomogeneity²³ leads to a strong local electric field and thus can reduce the threshold for the breakdown due to inter-LL scattering.

For $\nu = \pm 2$, V_{Hall} matches quite well with $\Delta E_{\nu=\pm 2}$, which indicates that the $n = 0$ LL width is small. However for $\nu = \pm 6, -10$, V_{Hall} is smaller than the corresponding cyclotron gap. This deviation for $\nu = \pm 6, -10$ can be explained by considering disorder-induced broadening of $n = \pm 1, -2$ LLs. The difference between ΔE_ν and eV_{Hall} is approximately ~ 35 meV (~ 415 K). These observations are consistent with the experiments measuring quantum Hall activation gap²⁴, which have also revealed similar width of these LLs in samples of similar mobilities. Additionally, the difference between V_{Hall} and ΔE_ν can also be attributed to inhomogeneous charge distribution. Considering inhomogeneous charge distribution, the critical current is predicted to be filling factor and length scale dependent¹³. However, the $n = 0$ level remains protected from the local electric field fluctuations^{13,25}. The correlation between V_{Hall} and ΔE_ν shows consistency with the breakdown mechanism based on this picture too. In addition, our experimental finding that there is a non-linear evolution of dissipation boundary can possibly be attributed to Hall field induced broadening of the extended state band.

To further explore the effect of transverse electric field, due to the high current density, we look at the plateau to plateau transition in transverse conductance (σ_{xy}). Fig.4 shows the $\nu = 2$ to $\nu = 6$ plateau transition at $T = 300$ mK and $B = 10$ T for different values of current. As we increase the injected current, the transition width starts to increase as well. Interestingly, in the transition region, all the curves intersect at the filling factor 4 and R_{xx} shows a small suppression in peak resistance around the same gate voltage (R_{xx} is shown in top-left inset).

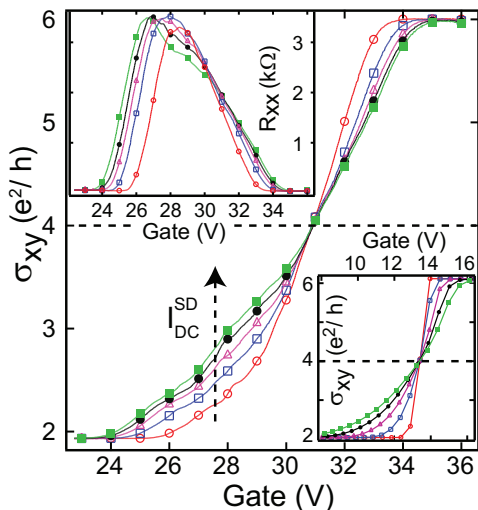


FIG. 4: (color online) Plot of σ_{xy} as a function of V_g for $\nu = 2$ to $\nu = 6$ plateau transition at $T = 300$ mK and $B = 10$ T for different values of currents starting from $0.75 \mu\text{A}$ with an increment of $1.5 \mu\text{A}$. The invariant point at $\nu = 4$ is clearly seen. The top-left inset shows the plot of R_{xx} as a function of V_g for the same transition at the same values of current as indicated in the main plot. The bottom-right inset shows the calculated values of σ_{xy} as a function of the V_g . The invariant point at $\nu = 4$ is also clearly seen.

Such an invariant point indicates that as we increase the current, the center of the electric field induced broadened extended state band does not move with the current. For $\nu = 2$ to $\nu = 6$ plateau transition, the Fermi level crosses the four fold degenerate $n = 1$ LL. It has been shown that at very high magnetic field, spin degeneracy can be lifted²⁶ giving rise to an additional plateau at $\nu = 4$. We speculate the current invariant point at $\nu = 4$ and suppression of R_{xx} at the same time as a precursor of Zee-

man splitting. To understand our data quantitatively, we carried out numerical calculations based on the injection model of QHE in graphene¹⁵. This model gives transverse conductance from the calculation of local density of states. The bottom-right inset in Fig.4 shows the conductance curves calculated for different values of the injected current. This model accurately describes the position of the current invariant point but fails to explain the width of the transition region. One possible reason for the failure of this model could be the assumption that all states are extended. Further detailed analysis is needed to take into account the effect of disorder.

In summary, we have studied the non-equilibrium breakdown of the quantum Hall state in graphene. We find that the dissipationless QH state can be suppressed due to a high current density, and the corresponding critical current decreases with $|\nu|$. The correlation between V_{Hall} and ΔE_ν is consistent with the disorder-induced broadening of LLs and inhomogeneous charge distribution. The value of V_{Hall} at breakdown gives an idea about the activation energy. Scanned probe based measurements on cleaner samples are likely to observe the electric field induced “collapse” ($\beta \geq 1$) of LLs. We also see a current invariant point in the plateau to plateau transition and suppression in longitudinal resistance at higher current, which can possibly be a sign of spin-degeneracy breakdown.

Acknowledgments

The authors would like to thank Hari Solanki, Sajal Dhara, Shamashis Sengupta, Prita Pant and Arnab Bhattacharya for their help. This work was supported by the Government of India.

* deshमुख@tifr.res.in
¹ *The Quantum Hall Effect*, edited by R.E. Prange and S.M. Girvin (Springer Verlag, New York, 1990), and references therein.
² G. Nachtwei, *Physica E*, **4**, 79 (1999), and references therein.
³ G. Ebert *et al.*, *J. Phys. C*, **16**, 5441 (1983)
⁴ S. Komiyama *et al.*, *Phys. Rev. Lett.*, **77**, 558 (1996).
⁵ O.G. Balev, and P. Vasilopoulos, *Phys. Rev. B.*, **47**, 16410 (1993).
⁶ P. Streda and K von Klitzing, *J. Phys. C*, **17**, L483 (1984)
⁷ L. Eaves, and F. W. Sheard, *Semicond. Sci. Technol.*, **1**, 346 (1986).
⁸ C. Chaubet *et al.*, *Semicond. Sci. Technol.*, **18**, 983 (2003).
⁹ R.F. Kazarinov, and S. Luryi, *Phys. Rev. B*, **25**, 7626 (1982).
¹⁰ V. Tsemekhman *et al.*, *Phys. Rev. B*, **55**, R10201 (1997).
¹¹ K. S. Novoselov *et al.*, *Nature*, **438**, 197 (2005); Y. Zhang *et al.*, *ibid.* **438**, 201 (2005).

¹² A. H. Castro Neto *et al.*, *Rev. Mod. Phys.*, **81**, 109 (2009) and references therein.
¹³ V. Lukose, R. Shankar, G. Baskaran, *Phys. Rev. Lett.*, **98**, 116802 (2007).
¹⁴ M.M. Nieto, and P. L. Taylor, *Am. J. Phys.*, **53**, 234 (1985).
¹⁵ T. Kramer *et al.*, cond-mat/0811.4595v2
¹⁶ K. S. Novoselov *et al.*, *Science*, **315**, 5817 (2007).
¹⁷ A. J. M. Giesbers *et al.*, *App. Phys. Lett.*, **93**, 222109 (2008).
¹⁸ Nominally, the filling factor is defined as the ratio of number of charge carriers to the number of magnetic flux quanta penetrating the sample and therefore is positive. However, in the context of QHE in graphene a negative filling factor is used to distinguish the filling factor of holes from that of electrons (cf.^{11,12}).
¹⁹ The $\nu = 10$ is not studied as the gate voltage required to study it can lead to a dielectric breakdown of the gate-dielectric SiO₂.

- ²⁰ E. H. Hwang, S. Adam, and S. Das Sarma, Phys. Rev. Lett., **98**, 186806 (2007).
- ²¹ A. A. Balandin *et al.*, Nano Lett., **8**, 902 (2008).
- ²² J.R. Kirtley *et al.*, Phys. Rev. B., **34**, R1384 (1986); **34**, 5414 (1986).
- ²³ J. Martin *et al.*, Nat. Phys., **4**, 144 (2008).
- ²⁴ A.J.M. Giesbers *et al.*, Phys. Rev. Lett., **99**, 206803 (2007).
- ²⁵ M. I. Katsnelson, Mater. Today, **10**, 20 (2007).
- ²⁶ Y. Zhang *et al.*, Phys. Rev. Lett. **96**, 136806 (2006).